

AD-A238 045

2

USAFSAM-TR-90-37



AUTOMATED RADIOFREQUENCY RADIATION DOSIMETRY

Om P. Gandhi, Sc.D.

Department of Electrical Engineering
The University of Utah
Salt Lake City, UT 84112

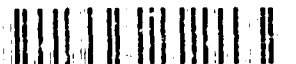


December 1990

Final Report for Period June 1989 - September 1990

Approved for public release; distribution is unlimited.

Prepared for
USAF SCHOOL OF AEROSPACE MEDICINE
Human Systems Division (AFSC)
Brooks Air Force Base, TX 78235-5301

91-04265





NOTICES


This final report was submitted by the Department of Electrical Engineering, University of Utah, Salt Lake City, Utah, under contract F33615-87-D-0609 Task 25, job order 7757-01-1Z with the USAF School of Aerospace Medicine, Human Systems Division, AFSC, Brooks Air Force Base, Texas. Mr. William D. Hurt (USAFSAM/RZP) was the Laboratory Project Scientist-in-Charge.

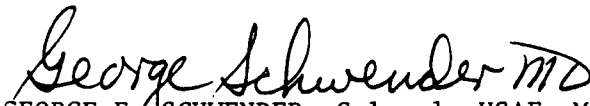
When Government drawings, specifications, or other data are used for any purpose other than in connection with a definitely Government-related procurement, the United States Government incurs no responsibility or any obligation whatsoever. The fact that the Government may have formulated or in any way supplied the said drawings, specifications, or other data, is not to be regarded by implication, or otherwise in any manner construed, as licensing the holder or any other person or corporation; or as conveying any rights or permission to manufacture, use, or sell any patented invention that may in any way be related thereto.

The Office of Public Affairs has reviewed this report, and it is releasable to the National Technical Information Service, where it will be available to the general public, including foreign nationals.

This report has been reviewed and is approved for publication.


WILLIAM D. HURT, M.S.
Project Scientist


DAVID N. ERWIN, Ph.D.
Supervisor


GEORGE E. SCHWENDER, Colonel, USAF, MC, CFS
Commander

REPORT DOCUMENTATION PAGE				Form Approved OMB No. 0704-0188	
1a. REPORT SECURITY CLASSIFICATION Unclassified		1b. RESTRICTIVE MARKINGS			
2a. SECURITY CLASSIFICATION AUTHORITY		3. DISTRIBUTION / AVAILABILITY OF REPORT Approved for public release; distribution is unlimited.			
2b. DECLASSIFICATION / DOWNGRADING SCHEDULE					
4. PERFORMING ORGANIZATION REPORT NUMBER(S)		5. MONITORING ORGANIZATION REPORT NUMBER(S) USAFSAM-TR-90-37			
6a. NAME OF PERFORMING ORGANIZATION Dept. of Electrical Engineering University of Utah		6b. OFFICE SYMBOL (if applicable)	7a. NAME OF MONITORING ORGANIZATION USAF School of Aerospace Medicine (RZP)		
6c. ADDRESS (City, State, and ZIP Code) Salt Lake City, UT 84112		7b. ADDRESS (City, State, and ZIP Code) Human Systems Division (AFSC) Brooks Air Force Base, TX 78235-5301			
8a. NAME OF FUNDING / SPONSORING ORGANIZATION		8b. OFFICE SYMBOL (if applicable)	9. PROCUREMENT INSTRUMENT IDENTIFICATION NUMBER F33615-87-D-0609 Task 25		
8c. ADDRESS (City, State, and ZIP Code)		10. SOURCE OF FUNDING NUMBERS			
		PROGRAM ELEMENT NO. 62202F	PROJECT NO. 7757	TASK NO. 01	WORK UNIT ACCESSION NO. 12
11. TITLE (Include Security Classification) Automated Radiofrequency Radiation Dosimetry					
12. PERSONAL AUTHOR(S) Gandhi, Om P.					
13a. TYPE OF REPORT Final		13b. TIME COVERED FROM 89/06 TO 90/09		14. DATE OF REPORT (Year, Month, Day) 1990, December	15. PAGE COUNT 30
16. SUPPLEMENTARY NOTATION					
17. COSATI CODES			18. SUBJECT TERMS (Continue on reverse if necessary and identify by block number)		
FIELD	GROUP	SUB-GROUP	Specific absorption rate distributions; Anatomically based human models; Finite-Difference Time-Domain Method; Improvement using expanding grid formulation; Adaptation of algorithm to		
06	07				
20	14				
19. ABSTRACT (Continue on reverse if necessary and identify by block number) The interaction of radiofrequency (RF) and microwave (MW) electromagnetic radiation with biological tissues is of increasing importance from the standpoint of health and safety. From considerable literature devoted to the study of RF and MW bioeffects based primarily on animal experimentation it has been determined that bioeffects are correlated with mass-normalized rates of RF or MW energy absorption (specific absorption rates or SARs). An emphasis of our project was to improve the efficiency of the SAR algorithms and to extend their use to higher RF and MW frequencies. Another objective was to adapt these algorithms to computing workstations and distributed memory parallel processors that are becoming more affordable and hence readily available to potential users of these codes.					
20. DISTRIBUTION / AVAILABILITY OF ABSTRACT <input checked="" type="checkbox"/> UNCLASSIFIED/UNLIMITED <input type="checkbox"/> SAME AS RPT. <input type="checkbox"/> DTIC USERS			21. ABSTRACT SECURITY CLASSIFICATION Unclassified		
22a. NAME OF RESPONSIBLE INDIVIDUAL William D. Hurt		22b. TELEPHONE (Include Area Code) (512) 536-2362		22c. OFFICE SYMBOL USAFSAM/RZP	

18. SUBJECT TERMS (Continued)

computing workstations; Coupling to EMP

19. ABSTRACT (Continued)

We have focused on the most promising of these algorithms based on the finite-difference time-domain (FDTD) method. With improved efficiency it has been possible to extend computations of SAR distributions from a 5628-cell anatomically based representation of the human body (cell size = 2.62 cm or nominal 1 in.) to a 45,024-cell representation (cell size = 1.31 cm or nominal 1/2 in.) and for a limited number of frequencies to a 360,192-cell representation of the human body (cell size = 0.655 cm or nominal 1/4 in.). Finer resolution of the model has permitted extension of calculations from the previous maximum frequency of 350 MHz to 915 MHz and with some approximations to 3,000 MHz. The FDTD algorithm has been adapted and used with the following workstations: Silicon Graphics IRIS, APOLLO RGB/DN 10,000, and IBM 520. A parallelized C-language version of the code has been developed and tested using a distributed memory transputer array consisting of 21 T-800/20 MHz processors.

The FDTD code has been used to calculate currents induced in the human body and the specific absorptions for the various organs for exposure to vertically polarized electromagnetic pulse (EMP) using both the 5628- and 45,024-cell representation of the human body. Also the code has been modified to allow a linearly expanding grid representation of the biological bodies. Allowing a high-resolution representation of the body surface including the eyes and the gonads, this latter improvement would be most helpful in extending the SAR calculations to microwave frequencies.

TABLE OF CONTENTS

	<u>Page</u>
INTRODUCTION	1
FINITE-DIFFERENCE TIME-DOMAIN METHOD	1
AN ANATOMICALLY BASED INHOMOGENEOUS MODEL OF THE HUMAN BODY.....	5
CURRENTS INDUCED IN THE HUMAN MODEL FOR EXPOSURE TO ELECTROMAGNETIC PULSE.....	5
SPECIFIC ABSORPTION RATE AND INDUCED CURRENT DISTRIBUTIONS FOR PLANE-WAVE EXPOSURES (100-915 MHz).....	8
MODIFICATION OF THE FDTD ALGORITHM -- LINEARLY EXPANDING GRID; UNEQUAL CELL SIDES.....	9
ADAPTATION OF THE FDTD CODE TO COMPUTING WORKSTATIONS	12
PARALLELIZATION OF THE FDTD CODE AND ITS IMPLEMENTATION ON A DISTRIBUTED MEMORY TRANSPUTER.....	16
WORK PROPOSED FOR NEXT YEAR.....	16
CONCLUDING REMARKS.....	18
MANUSCRIPT ACCEPTED FOR PUBLICATION.....	19
MANUSCRIPTS IN PREPARATION.....	19
REFERENCES.....	20

Accession For	
NTIS GRA&I	<input checked="" type="checkbox"/>
DTIC TAB	<input type="checkbox"/>
Unannounced	<input type="checkbox"/>
Justification	
By	
Distribution/	
Availability Codes	
Dist	Avail and/or Special
A-1	

Figures

<u>Fig. No.</u>		<u>Page</u>
1	A unit cell of the Yee lattice indicating the positions for the various field components.	2
2	Fourier Spectrum of the EMP-induced current for the section through the knees (fairly similar Fourier Spectra have also been obtained for currents for the sections through ankles, thighs, heart, neck, etc.).....	8
3	Part-body-averaged SARs for the various regions of the body for an incident E-polarized power density of 1 mW/cm ² . Frequency band 100-915 MHz.	10
4	Average SARs for the various organs of the body for an incident E-polarized power density of 1 mW/cm ² . Frequency band 100-915 MHz.	11
5	Comparison of the E-fields calculated from linearly expanding grid FDTD algorithm with the analytic results [26] for the various cuts of a lossy muscle-equivalent sphere at 3,000 MHz ($k_0 a = 6.6$). Diameter of the sphere = 21 cm (corresponding to the dimension of the human head). Taken from reference 23, dielectric properties of the sphere are $\epsilon_r = 46$, $\sigma = 2.26$ S/m. Expansion factors along the three axes are: $\alpha_x = \alpha_z = 1.08$, $\alpha_y = 1.05$	13

Tables

<u>Table No.</u>		
1	Tissue properties used at some representative frequencies.	6

AUTOMATED RADIOFREQUENCY RADIATION DOSIMETRY

INTRODUCTION

The interaction of radiofrequency (RF) and microwave (MW) electromagnetic (EM) radiation with biological tissues is of increasing importance from the standpoint of health and safety. There is considerable literature devoted to the study of RF and MW bioeffects based on both animal experimentation and theoretical models. Typically bioeffects are correlated with mass-normalized rates of RF or MW energy absorption (specific absorption rates (SARs)) expressed in watts per kilogram (W/kg).

The American National Standards Institute (ANSI) has issued a guidance standard [1] for radiofrequency radiation (RFR) exposure level needed to cause behavioral effects in laboratory animals. This standard is based on a threshold whole-body-averaged SAR of 4 W/kg. The ANSI guidance standard incorporates a safety factor of 10, hence whole-body-averaged SAR levels below 0.4 W/kg averaged over a 6-min period are considered safe. Recognizing the highly nonuniform nature of SAR distribution, including some regions where there may be fairly high local SARs, the ANSI standard further stipulates that local SAR in any 1 g of tissue must not exceed 8 W/kg.

The main focus of our project has been to develop anatomically based EM models of the human body to obtain quantitative information on SARs for the various parts of the body for exposure to RFR for a variety of exposure conditions. Another thrust of this project was to adapt the numerical SAR algorithms to computing workstations and to distributed memory parallel processors that are becoming more affordable and hence more readily available to many potential users of these codes.

FINITE-DIFFERENCE TIME-DOMAIN METHOD

The most promising of the methods for calculation of SAR distributions at the present time is the finite-difference time-domain (FDTD) method [2-8]. This method was first proposed by Yee [9] and later developed by Taflove and colleagues [10-12], Umashankar and Taflove [13], Holland [14], and Kunz and Lee [15]. Recently it has been extended for calculations of the distribution of electromagnetic fields (EMF) in a man model for incident plane waves [2-6] and for exposures in the near fields [7, 8]. In this method, the time-dependent Maxwell's curl equations

$$\nabla \times \mathbf{E} = -\mu \frac{\partial \mathbf{H}}{\partial t} \quad , \quad \nabla \times \mathbf{H} = \sigma \mathbf{E} + \epsilon \frac{\partial \mathbf{E}}{\partial t} \quad (1)$$

are implemented for a lattice of cubic cells. The components of \mathbf{E} and \mathbf{H} are positioned about a unit cell of the lattice (Figure 1) and evaluated alternately with half-time steps. The goal of the method is to model the propagation of an EM wave into a volume of space containing dielectric and/or conducting structures by time stepping, i.e., repeatedly implementing a finite-difference analog of the curl equations at each cell of the corresponding space lattice. The incident wave is tracked as it first propagates to the dielectric structure and interacts with it via surface current excitation, spreading, penetration, and diffraction. Wave tracking is completed when a sinusoidal

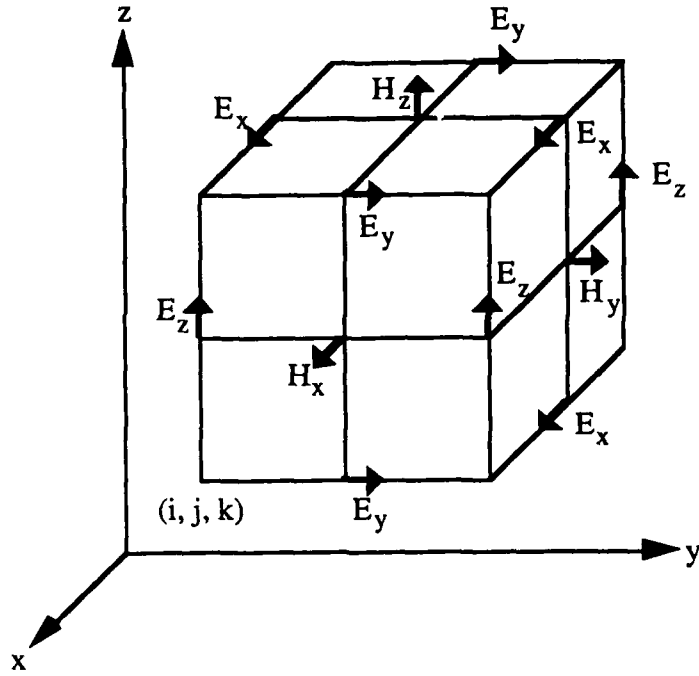


Figure 1. A unit cell of the Yee lattice indicating the positions for the various field components.

steady-state behavior for \mathbf{E} and \mathbf{H} fields is observed for each lattice cell. A second approach is to illuminate the body with a pulse of radiation in the time domain. If the medium is nondispersive (i.e., its dielectric properties do not change with frequency), this method has the advantage of giving the performance of the medium at various frequencies from the inverse Fourier transform of the calculated fields. Though Spiegel and his collaborators [2-3] have followed this approach, we have used the sinusoidal variation of the illuminating fields since the dielectric properties of the tissues are highly dependent on frequency.

The Maxwell's equations (1) can be rewritten as difference equations. We assume the media to be nonmagnetic, i.e., $\mu = \mu_0$ and a grid point of the space defined as (i, j, k) with coordinates $(i\delta, j\delta, k\delta)$ where δ is the cell size.

Upon substituting

$$\tilde{\mathbf{E}} = \sqrt{\frac{\epsilon_0}{\mu_0}} \frac{\mathbf{E}}{2} \quad (2)$$

the equations in difference form for \mathbf{E}_z and \mathbf{H}_z , for examples, can be written as:

$$\tilde{E}_z^{n+1}(i, j, k + 1/2) = CA_z(i, j, k + 1/2) \tilde{E}_z^n(i, j, k + 1/2) +$$

$$CB_z(i, j, k + 1/2) \bullet \left[\begin{array}{l} H_y^{n+1/2}(i + 1/2, j, k + 1/2) - H_y^{n+1/2}(i - 1/2, j, k + 1/2) \\ + H_x^{n+1/2}(i, j - 1/2, k + 1/2) - H_x^{n+1/2}(i, j + 1/2, k + 1/2) \end{array} \right] \quad (3)$$

$$H_z^{n+1/2}(i + 1/2, j + 1/2, k) = H_z^{n-1/2}(i + 1/2, j + 1/2, k)$$

$$+ \left[\begin{array}{l} \bar{E}_x^n(i + 1/2, j + 1, k) - \bar{E}_x^n(i + 1/2, j, k) \\ + \bar{E}_y^n(i, j + 1/2, k) - \bar{E}_y^n(i + 1, j + 1/2, k) \end{array} \right] \quad (4)$$

where

$$CA_z(i, j, k + 1/2) = \left[1 - \frac{\sigma_z(i, j, k + 1/2) \delta t}{2\epsilon_z(i, j, k + 1/2)} \right] \left[1 + \frac{\sigma_z(i, j, k + 1/2) \delta t}{2\epsilon_z(i, j, k + 1/2)} \right]^{-1} \quad (5)$$

$$CB_z(i, j, k + 1/2) = \frac{\epsilon_0}{4} \left[\epsilon_z(i, j, k + 1/2) + \frac{\sigma_z(i, j, k + 1/2) \delta t}{2} \right]^{-1} \quad (6)$$

where the superscript n denotes the time n δt in terms of the incremental time or time step δt . The time step δt is determined by the cell size and must satisfy the stability condition [10]

$$v_{\max} \delta t < \left[\frac{1}{\delta x^2} + \frac{1}{\delta y^2} + \frac{1}{\delta z^2} \right]^{-1/2} \quad (7)$$

where v_{\max} is the maximum wave phase velocity within the model. For the cubic cell model $\delta x = \delta y = \delta z = \delta$, the following relationship is usually taken

$$\delta t = \frac{\delta}{2v_{\max}} \quad (8)$$

where v_{\max} is the maximum velocity of EM waves in the interaction space. We have taken v_{\max} corresponding to velocity of EM waves in air. The ϵ and σ may be different for E_x , E_y , and E_z in

the inhomogeneous media, because, as shown in Figure 1, the components of \mathbf{E} are not positioned at the same point for the same cell in Yee's algorithm. Thus we have $\epsilon_x, \epsilon_y, \epsilon_z, \sigma_x, \sigma_y,$ and σ_z for each of the cells.

A basic problem with any finite-difference solution of Maxwell's equations is the treatment of the field components at the lattice truncation. Because of the limited computer storage, the lattice must be restricted in size. Proper truncation of the lattice requires that any outgoing wave disappear at the lattice boundary without reflection during the continuous time stepping of the algorithm. An absorption boundary condition for each field component is therefore needed at the edge of the lattice. In our formulation, the absorption boundary conditions in second approximation derived by Mur [16] are used. The condition for E_z at $i = 1$, for example, can be written as:

$$\begin{aligned} \tilde{E}_z^{n+1}(1, j, k + 1/2) = & -\tilde{E}_z^{n-1}(2, j, k + 1/2) \\ & + \frac{C_z \delta t - \delta}{C_z \delta t + \delta} \left[\tilde{E}_z^{n+1}(2, j, k + 1/2) + \tilde{E}_z^{n-1}(1, j, k + 1/2) \right] \\ & + 2 \left(\frac{\delta}{C_z \delta t + \delta} - \frac{(C_z \delta t)^2}{\delta(C_z \delta t + \delta)} \right) \left(\tilde{E}_z^n(1, j, k + 1/2) + \tilde{E}_z^n(2, j, k + 1/2) \right) \\ & + \frac{(C_z \delta t)^2}{2\delta(C_z \delta t + \delta)} \left[\begin{aligned} & \tilde{E}_z^n(1, j + 1, k + 1/2) + \tilde{E}_z^n(1, j - 1, k + 1/2) + \tilde{E}_z^n(2, j + 1, k + 1/2) \\ & + \tilde{E}_z^n(2, j - 1, k + 1/2) + \tilde{E}_z^n(1, j, k + 3/2) + \tilde{E}_z^n(1, j, k - 1/2) \\ & + \tilde{E}_z^n(2, j, k + 3/2) + \tilde{E}_z^n(2, j, k - 1/2) \end{aligned} \right] \quad (9) \end{aligned}$$

where C_z is the phase velocity of the medium at the lattice truncation.

As a part of this project, several steps have been taken to improve the efficiency of the FDTD code. Since a major problem with this code is the large amount of memory storage that is needed, we have reduced the parameters that need to be stored. First, $\sigma_x, \sigma_y, \sigma_z$ and $\epsilon_x, \epsilon_y,$ and ϵ_z that were previously stored for all N cells at half-cell intervals have been replaced by single volume-averaged values of σ and ϵ for each of the cells, resulting in considerable reduction in the number of parameters that need to be stored. This step has also resulted in the intermediate property-dependent quantities such as $CA_x, CB_x, CA_y, CB_y, CA_z,$ and CB_z being replaced by CA and CB for each of the cells -- leading once again to a considerable reduction in memory. The steps taken to date have reduced the memory storage requirement by roughly one half and computation time for a typical run for $N = 100,000$ cells using CRAY XMP from 8 to 5 min.

With these memory and time-saving steps taken, the test runs for currents induced in the human body for exposure to electromagnetic pulse (EMP) have shown negligible difference in the results.

AN ANATOMICALLY BASED INHOMOGENEOUS MODEL OF THE HUMAN BODY

As previously described in Sullivan *et al.* [4, 5], the model for the human body is developed from information in the book, *A Cross-Section Anatomy*, by Eycleshymer and Schoemaker [17]. This book contains cross-sectional diagrams of the human body which were obtained by making cross-sectional cuts at spacing of 2.54 cm (1 in.) in human cadavers. The process for creating the data base of the man model was the following: first of all, a 0.635-cm (1/4 in.) grid was taken for each single cross-sectional diagram and each cell on the grid was assigned a number corresponding to 1 of the 14 tissue types given in Table 1, or air. Thus the data associated with a particular layer consisted of three numbers for each square cell: x and y positions relative to some anatomical reference point in this layer, usually the center of the spinal cord, and an integer indicating which tissue that cell contained. Since the cross-sectional diagrams available in Eycleshymer and Schoemaker [17] are for somewhat variable separations, typically 2.3-2.7 cm, a new set of equispaced layers were defined at 0.635-cm (1/4 in.) intervals by interpolating the data onto these layers. Because the cell size of 0.635 cm results in a model with a large number of cells that is difficult to accommodate in the memory space of commonly available computers, the proportion of each tissue type was calculated next for somewhat larger cells of size 1.27 cm (1/2 in.) or 2.54 cm (1 in.) combining the data for $2 \times 2 \times 2 = 8$ or $4 \times 4 \times 4 = 64$ cells of the smaller dimension. Without changes in the anatomy, this process allows some variability in the height and weight of the body. We have taken the final cell size of 1.31 or 2.62 cm (rather than 1/2 in. or 1 in.) to obtain the whole-body weight of 69.6 kg for the model. The number of cells either totally or partially within the human body for the two models are 45,024 and 5,628, respectively.

CURRENTS INDUCED IN THE HUMAN MODEL FOR EXPOSURE TO ELECTROMAGNETIC PULSE

Though not assigned as a task on this project, we have used the FDTD method to calculate the internal fields and the induced current densities in anatomically based models of the human body with 5,628 or 45,024 cubical cells of dimensions 2.62 and 1.31 cm, respectively, for exposure to EMP. High-intensity electric and magnetic fields associated with an EMP have resulted in a need to understand its coupling to the human body to assess potential health effects. Electric fields as high as 50-100 kV/m and magnetic fields that are approximately 1/377 times lower have been measured close to EMP generators. The fields are, of course, considerably lower at larger distances from these generators. The EMPs are marked by rise times on the order of 10-30 ns with pulse durations on the order of 100-300 ns.

Approximating the human body by 3 cylinders of uniform conductivity, 1 vertical and 2 horizontal to represent shoulders, Grønhaug has calculated currents induced for exposure to an EMP [18]. Guy, on the other hand, has used a model consisting of 12 cylindrical sections each representing approximately 15-cm (5.9 in.) height of the human body [19]. These sections are loaded with parallel resistance-capacitance (RC) circuits representing the measured impedance for a human subject for the corresponding sections of the body. Approximating the incident EMP by an expression $E(t) = K[e^{\alpha t} - e^{\beta t}]$, currents for various frequency components (75 frequencies covering the range 100 Hz to 300 MHz) are calculated using the NEC 2D code detailed in Burke and Poggio [20]. The induced current in the time domain for the minimum area section representing the feet and ankles is then obtained from the Fourier transform of the currents calculated for the various frequencies.

TABLE 1. TISSUE PROPERTIES USED AT SOME REPRESENTATIVE FREQUENCIES

Tissue Type	Mass density 1,000 kg/m ³	27.12 MHz		100 MHz		350 MHz	
		$\sigma_{S/m}$	ϵ_r	$\sigma_{S/m}$	ϵ_r	$\sigma_{S/m}$	ϵ_r
Air	0.0012	0.0	1.0	0.0	1.0	0.0	1.0
Muscle	1.05	0.74	106	1.0	74	1.33	53.0
Fat, bones	1.20	0.04	29	0.07	7.5	0.072	5.7
Blood	1.00	0.28	102	1.1	74	1.2	65.0
Intestines	1.00	0.29	60	0.55	36	0.66	26.5
Cartilage	1.00	0.04	29	0.07	7.5	0.072	5.7
Liver	1.03	0.51	132	0.62	77	0.82	50.0
Kidney	1.02	0.79	209	1.0	90	1.16	53.0
Pancreas	1.03	0.69	206	1.0	90	1.16	53.0
Spleen	1.03	0.69	206	0.82	100	0.9	90.0
Lung	0.33	0.17	34	0.34	75	1.1	35.0
Heart	1.03	0.64	210	0.75	76	1.0	56.0
Nerve, brain	1.05	0.45	155	0.53	52	0.65	60.0
Skin	1.00	0.74	106	0.55	25	0.44	17.6
Eye	1.00	0.45	155	1.9	85	1.9	80.0

Since these models are fairly gross approximations, we have used the anatomically based model of a human to calculate currents induced in the human body for exposure to a few representative EMPs. The FDTD technique [5-7] was used to calculate the internal fields (E) and the current densities (J) for each of the cubical cells of dimensions 2.62 cm (5,628 cells) or 1.31 cm (45,024 cells) that are used to describe the human body. As previously described [5-7], the volume-averaged dielectric properties and mass densities were obtained from the contents of these subvolumes in terms of the 16 tissues and air. The information on the tissue contents were obtained with a resolution of 0.635 cm (1/4 in.) from the anatomical diagrams [17]. The models were assumed with a layer of dielectric constant $\epsilon_r = 4.2$ of thickness 2.62 cm under the feet to simulate a human wearing rubber-soled shoes. This assumed thickness corresponds to the width of 1 or 2 cells for the 2 models, respectively.

Being a time-domain technique, the FDTD method is ideally suited for calculations involving EMP. Exact pulse shapes can be modeled by using small time increments. This method does, however, require that the dielectric properties of the body be nondispersive, i.e., independent of frequency in the band representing the frequency content of the EMP. This requirement, unfortunately, is not met for the human tissues which are known to be dispersive. A rigorous approach to this problem using the FDTD would therefore require the solution of Maxwell's equations coupled to the polarization equations in the time domain for the various tissues. Since the scope of the present project did not call for a full-blown effort in this regard, we have used an approximate model that uses the dielectric properties at 40 MHz. This approach is somewhat justified since the predominant components of the induced current are at frequencies close to 40-50 MHz, which is near the resonant frequency of an adult human standing on a ground plane [21].

The total induced currents for the various sections of the body and the specific absorptions for several organs are given by Chen and Gandhi [31] for two representative EMPs. The calculated results for the induced currents are compared with the data measured for a human subject (measured data courtesy of Mr. Wayne Hammer, Naval Surface Warfare Center, White Oak, Maryland). The calculated results are in excellent agreement with the measured data albeit for one human subject to date.

Using the graphics available with the IBM model 520 workstation, the staff at IBM, Salt Lake City, has helped us create a movie of EMP interaction with a nominal 1-in. model of the human body (actual cell size = 2.62 cm). Since software was not available to transfer the computer movie onto a videotape, pictures of sequential frames of this movie were used for our presentation, "Current Induced in an Anatomically Based Model of a Human for Exposure to Vertically Polarized EMP," at the Twelfth Annual Meeting of the Bioelectromagnetics Society, June 10-14, 1990, in San Antonio, Texas.

We have also developed a simplified procedure to calculate the coupling of the EMP to the human body. In this procedure the response of the human model is calculated for a narrow impulse (width of 0.218 ns) of RFR. The calculated current variations for the various sections of the body (such as sections through the ankles, knees, thighs, bladder, heart, neck, eyes, and others) are stored on a computer diskette. By convolving the calculated impulse response with a prescribed EMP in the time domain, we can get the currents for these same sections of the body that would have been induced as a result of this EMP. This procedure has been tested with an EMP provided by the ALECS facility, Kirtland Air Force Base, New Mexico (Figure 4 [31]). The current variations obtained for the various sections using this simplified procedure are identical to those shown in Figure 6a-e of Chen's and Gandhi's manuscript [31], the latter having been derived by the exact method. Since the convolution integral is a relatively simple step that can be carried out with a personal computer (PC), the response of the human body can thus be obtained for any EMP once the computer run for the impulse response has been made and data supplied on a diskette.

Further evaluation of the previous calculations for EMP [31] have also revealed a problem. Shown in Figure 2 is the Fourier Spectrum of the current induced for the section through the knees taken from Figure 6b of Chen's and Gandhi's report [31]. Fairly similar Fourier Spectra have also been obtained for other sections of the body. The broad bandwidth of the current components (~0-70 MHz) casts doubt on the validity of having assumed frequency-independent properties ϵ and σ corresponding only to 40 MHz, since the properties over the pertinent region of frequencies can change by a factor of 2:1 or more. An approach to resolve this problem will be to obtain time-domain formulations of the tissue properties ϵ and σ from the known frequency-domain variations and use these to calculate the impulse response which can then be convolved with the prescribed EMPs. This approach has, however, yet to be tried and tested for accuracy.

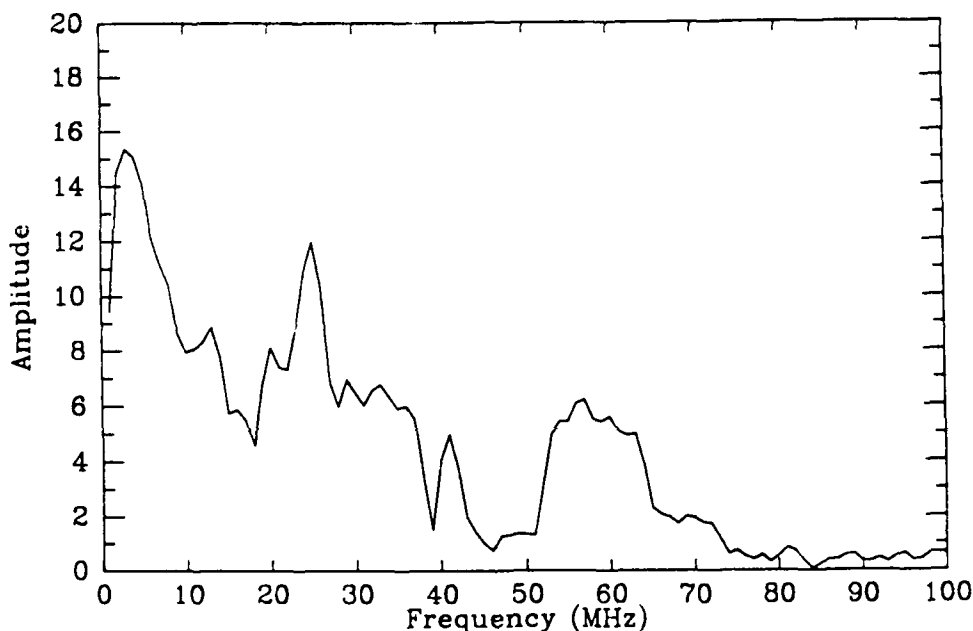


Figure 2. Fourier Spectrum of the EMP-induced current for the section through the knees (fairly similar Fourier Spectra have also been obtained for currents for the sections through ankles, thighs, heart, neck, and others).

SPECIFIC ABSORPTION RATE AND INDUCED CURRENT DISTRIBUTIONS FOR PLANE-WAVE EXPOSURES (100-915 MHz)

We had previously used the FDTD method to calculate local, layer-averaged, and whole-body-averaged SARs and internal RF currents in a 5,628-cell (cell size = 2.62 cm) anatomically based model of the human body for plane-wave exposure 20-100 MHz [6].

Using the finer resolution (cell size = 1.31 cm), 45,024-cell representation of the human body, calculations have recently been extended to frequencies of 120-200 MHz in 10-MHz steps and frequencies of 225, 250, 300, 350, 500, 700, and 915 MHz. Frequency-dependent properties for the various tissues were taken from the literature [22, 23]. This work is described in detail in the report by Gandhi *et al.* [32]. Special attention was given to the frequency band 120-200 MHz to see if we could predict the high SARs that had been observed for the neck by Stuchly *et al.* [24] at 160 MHz using a four-tissue (skeleton, brain, lungs, and muscle) heterogeneous model of man.

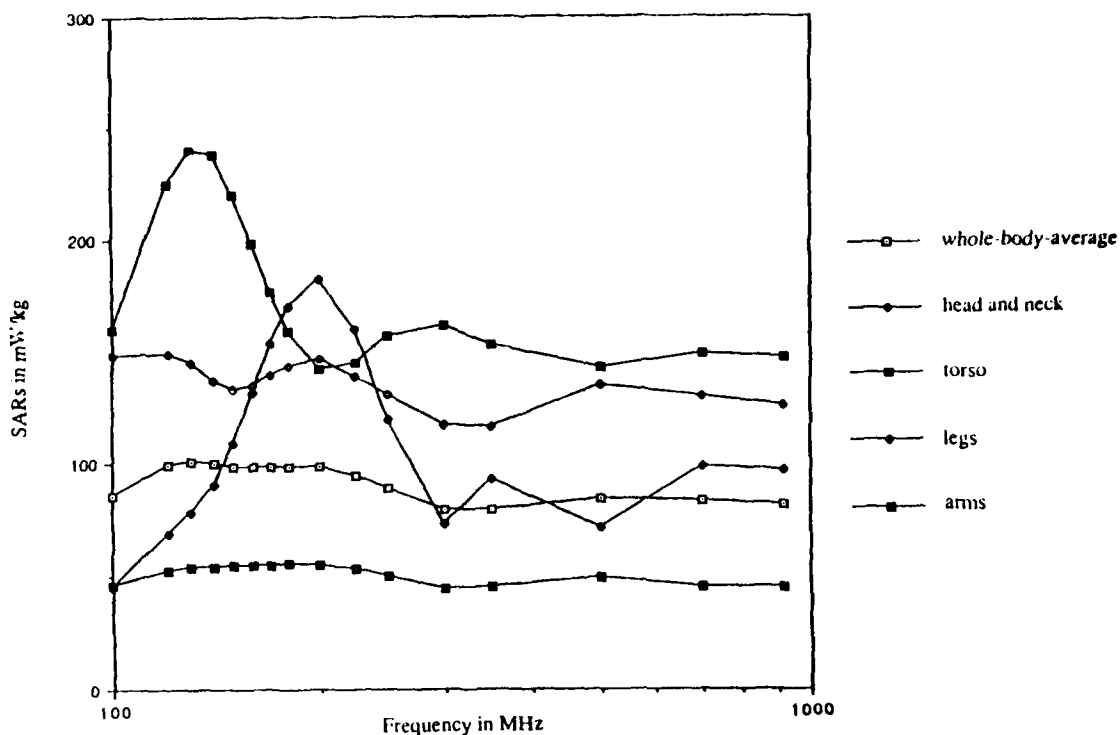
In the work by Stuchly *et al.* [24] only three frequencies -- 160, 350, and 915 MHz -- and isolated human model had been studied. By taking a closer frequency interval of 10 MHz in the band 120-200 MHz, we wanted to pinpoint the frequencies for maximum SARs in the neck both for isolated and grounded conditions of the model. From our calculations for the **isolated** human model (irradiation condition used by Stuchly *et al.* [24]), the highest layer-averaged SAR is found for the neck section not at 160 MHz used as one of the irradiation frequencies by these authors (the other two irradiation frequencies were 350 and 915 MHz), but rather at 200 MHz. The maximum layer-averaged SAR for the neck section at 200 MHz has the value 0.55 W/kg for an incident power density of 1 mW/cm². Since only local values are given for 38 locations in the body in the article by Stuchly *et al.* [24], data was not available for comparison with the layer-averaged SARs calculated at 160 MHz or for any of the other 15 frequencies used in our calculations. The highest local SAR calculated for the center of the neck is 3.22 W/kg at 200 MHz. This value is considerably higher than about 1.8 W/kg that was measured for this general region by Stuchly *et al.* [24] at 160 MHz using their four-tissue heterogeneous model (skeleton, brain, lungs, and muscle). The peak value for the center of the neck in our 16-tissue anatomically based model at 160 MHz is 2.41 W/kg. This value compares favorably with 1.8 W/kg measured for this general location by Stuchly *et al.* [24] when one realizes that only a four-tissue phantom was used by these authors. While no reason was offered by Stuchly *et al.* [24] for the high SARs observed in the neck at 160 MHz, we find that the peak RF induced currents both for isolated and grounded conditions shift to the upper half of the body for frequencies in the band 120-300 MHz (see Figure 9b- ℓ of [32]) rather than the lower parts of the body and the legs as previously reported for frequencies smaller than 100 MHz [6, 25]. Because of the smaller cross-sectional area of the neck, highest layer-averaged and local SARs are therefore calculated for the neck section.

We have also used the calculated SAR distributions to obtain part-body (head and neck, torso, legs, and arms) and organ-averaged SARs (eyes, brain, heart, lungs, liver, kidneys, intestines). Taken from the report by Gandhi *et al.* [32], the part-body and organ-averaged SARs are given in Figures 3 and 4, respectively. The highest part-body-averaged SAR for the head and neck region for the isolated condition of the model occurs at 200 MHz where the SAR for this region of the body is 182.5 mW/kg.

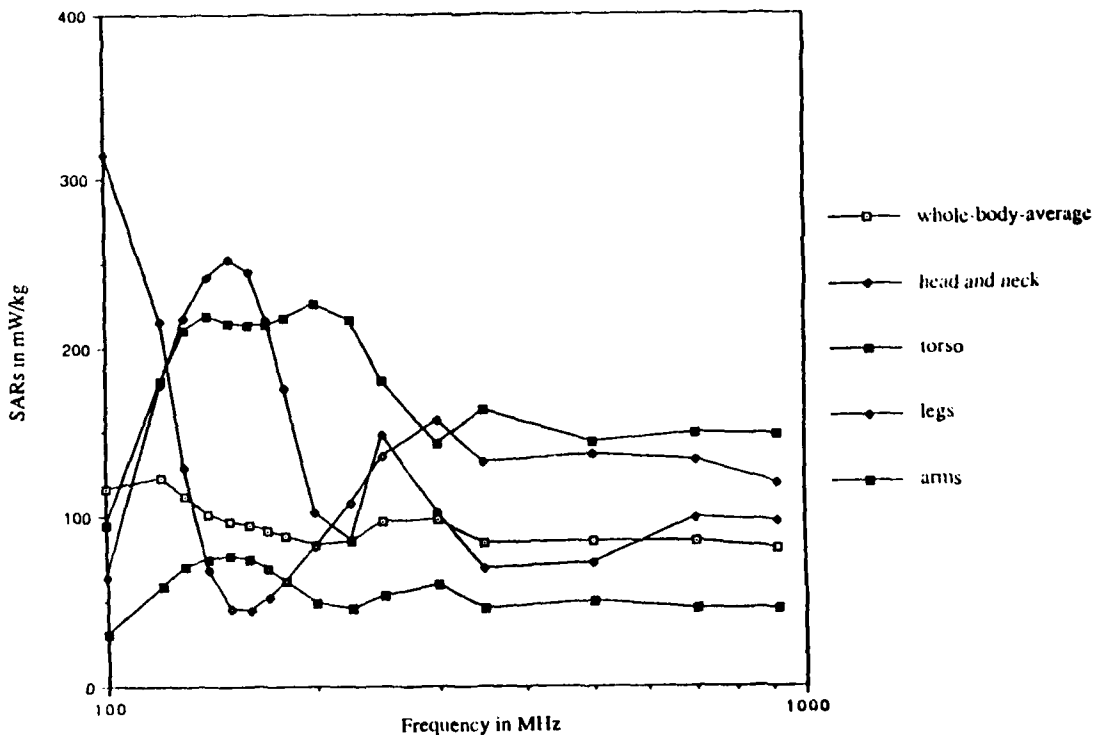
In Figures 4a and b we have plotted the averaged SARs calculated for the various organs in the body for isolated and grounded conditions of the model, respectively. The organs considered are brain, eyes, heart, lungs, liver, kidneys, and intestines. In the frequency band 100-200 MHz the highest SARs for the eyes and the brain occur for frequencies that coincide with the highest absorption frequencies in the head and neck region. The highest absorption frequencies for the eyes and the brain (as well as the head and neck region) are 200 and 150 MHz for isolated and grounded model conditions, respectively. Because of the increasingly superficial nature of EM deposition at higher frequencies, the average SARs for the eyes and the brain also rise for frequencies above 350 MHz.

MODIFICATION OF THE FDTD ALGORITHM -- LINEARLY EXPANDING GRID; UNEQUAL CELL SIDES

Recognizing that the EM deposition at microwave frequencies is primarily superficial, e.g., in the eyes, the frontal lobe of the brain, gonadal area, and others, we have modified the FDTD algorithm to use a linearly expanding grid rather than a uniform grid that has always been used in the past for this method. The expanding grid algorithm allows cell-to-cell expansion factors that can be different along the three axes. Expansion factors α on the order of 1.03 to 1.08 have been found to give results that are in excellent agreement with those obtained analytically for two-dimensional (2-D) homogeneous and layered cylinders and for three-dimensional (3-D) homogeneous spheres [26]. Because of the power of compounding, the cell size after n -cells is $\delta_{\min} \alpha^n$ where δ_{\min} is the minimum cell size for the grid. This size can be considerably larger than the

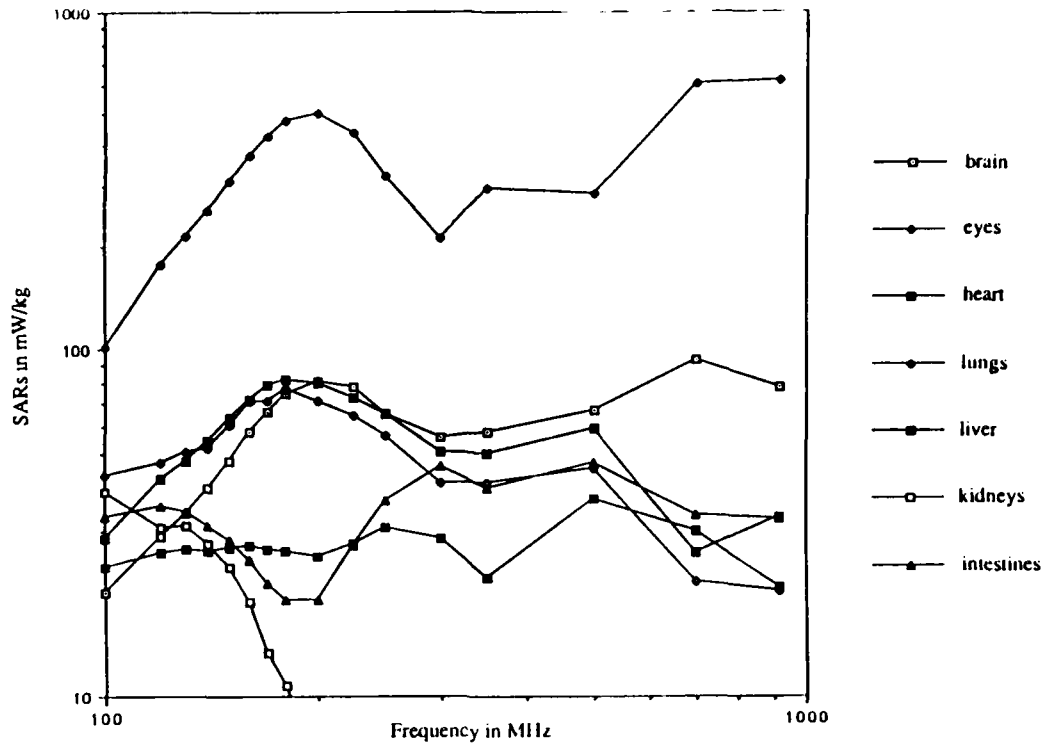


a. Isolated Model

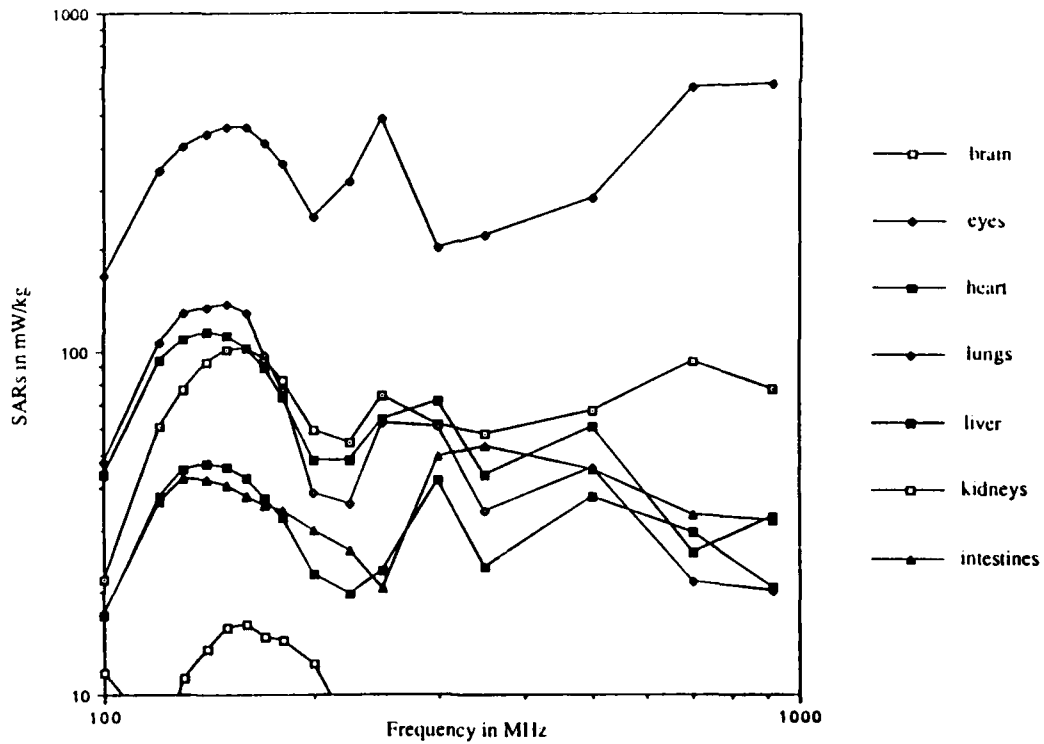


b. Grounded Model

Figure 3. Part-body-averaged SARs for the various regions of the body for an incident E-polarized power density of 1 mW/cm^2 . Frequency band 100-915 MHz.



a. Isolated Model



b. Grounded Model

Figure 4. Average SARs for the various organs of the body for an incident E-polarized power density of 1 mW/cm^2 . Frequency band 100-915 MHz.

minimum cell size that is used. In air outside the body, such larger cell sizes are obviously acceptable and are still much smaller than $\lambda_0/10$ where λ_0 is the wavelength in air. In the interior of the body these larger cell sizes are also acceptable since the SAR is fairly negligible. A comparison of the fields calculated with expanding grid algorithm and the analytical series solution [26] for a lossy dielectric sphere ($\epsilon_r = 46$, $\sigma = 2.26$ S/m) of diameter 21 cm (8.4 in.) at 3,000 MHz along various cuts of the body is given in Figure 5. The agreement can be seen to be fairly good. Fairly excellent agreements have also been observed for this sphere at other frequencies up to 3,000 MHz.

We have also modified the FDTD algorithm so that it is possible to use **different cell sizes along the three axes**. In future studies it should be possible to use parallelepiped rather than cubical cells, allowing a degree of flexibility that may be helpful in some applications.

ADAPTATION OF THE FDTD CODE TO COMPUTING WORKSTATIONS

A major task on the project was to adapt the FDTD code to computing workstations that are becoming more affordable and hence more readily available to many potential users of these codes. As a part of this project the FDTD code has been adapted and used with the following workstations: Silicon Graphics IRIS (memory 12 Mbytes), APOLLO RGB/DN 10,000 (memory 64 Mbytes), and IBM 520 (64 Mbytes). In addition to the nominal 1-in and 1/2-in models that we have used for the results described in the earlier sections, a nominal 1/4-in.-resolution (actual cell size = 6.55 mm), anatomically based model of the human body has been recently created from the data base that was previously used for the coarser models. This model is nested in an interaction space of $285 \times 110 \times 62 = 1,943,700$ or nearly 2 million cells. This is the first time that a human body model with such a high resolution has been run anywhere. For preliminary runs we have assumed plane wave exposures at 915, 1,500, 2,450, and 3,000 MHz and have used the tissue properties at the corresponding frequencies. APOLLO 10,000 Workstation has been used for calculations of SAR distributions. Total computation times for the various frequencies are as follows: 8 h at 915 MHz; 5 h, 20 min at 1,500 MHz; 4 h, 40 min at 2,450 MHz; and about 4 h at 3,000 MHz. Because of the need to cover about four periods of the incident wave to obtain convergence and the fact that the time step $\delta t = \delta/2c = 0.0109$ ns is dependent only on the cell size and not on frequency, fewer iterations are needed at higher frequencies -- hence the diminishing computation time at these frequencies.

Since the data base for the 1/4-in. model is less than satisfactory having been obtained by interpolation from anatomical sections that for the previous models were available only for separations on the order of 2.3-2.7 cm, it is obvious that a better model is needed before the higher frequency results are taken seriously. Also we need to increase the separation to the absorbing boundaries, which would require a somewhat larger number of cells for the interaction space. We may, of course, be able to move the absorbing boundary behind the model closer to, and perhaps within, the body since the fields at these locations are negligible, particularly at the higher frequencies.

To sum up, models of the human body and the surrounding space (needed for truncation of the FDTD code) used to date have the following number of cells:

$$84 \times 38 \times 26 = 82,992 \text{ cells (cell size} = 2.62 \text{ cm, nominal 1")}$$

$$163 \times 76 \times 52 = 644,176 \text{ cells (cell size} = 1.31 \text{ cm, nominal 1/2")}$$

$$285 \times 110 \times 62 = 1,943,700 \text{ cells (cell size} = 0.655 \text{ cm, nominal 1/4")}$$

The memory requirements for these models and the workstations used to date are as follows:

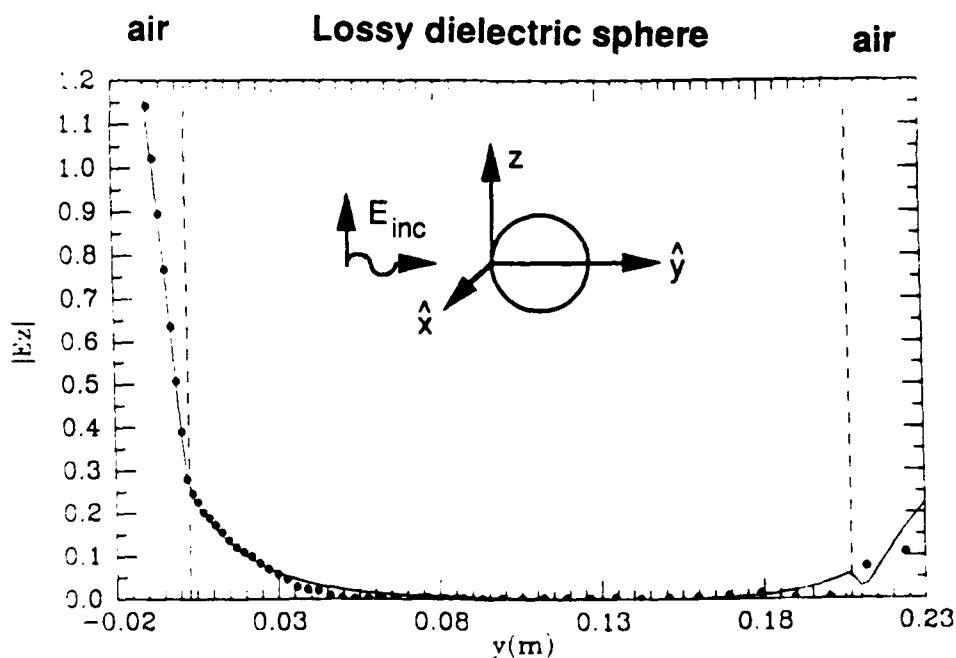
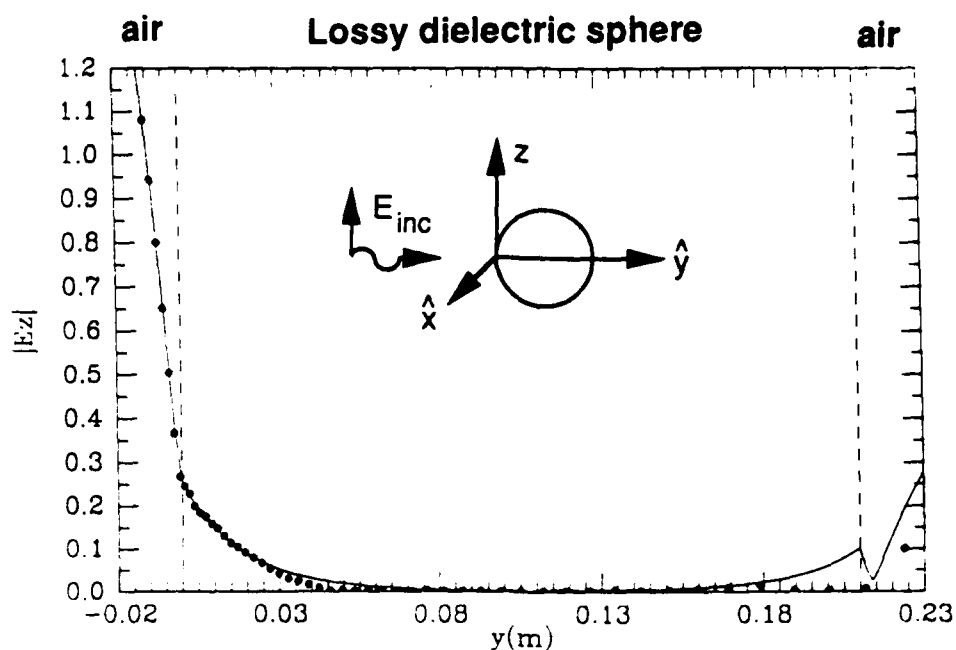


Figure 5. Comparison of the E-fields calculated from linearly expanding grid FDTD algorithm with the analytic results [26] for the various cuts of a lossy muscle-equivalent sphere at 3.000 MHz ($k_0 a = 6.6$). Diameter of the sphere = 21 cm (corresponding to the dimension of the human head). Taken from reference 23, dielectric properties of the sphere are $\epsilon_r = 46$, $\sigma = 2.26$ S/m. Expansion factors along the three axes are: $\alpha_x = \alpha_y = 1.08$, $\alpha_z = 1.05$.

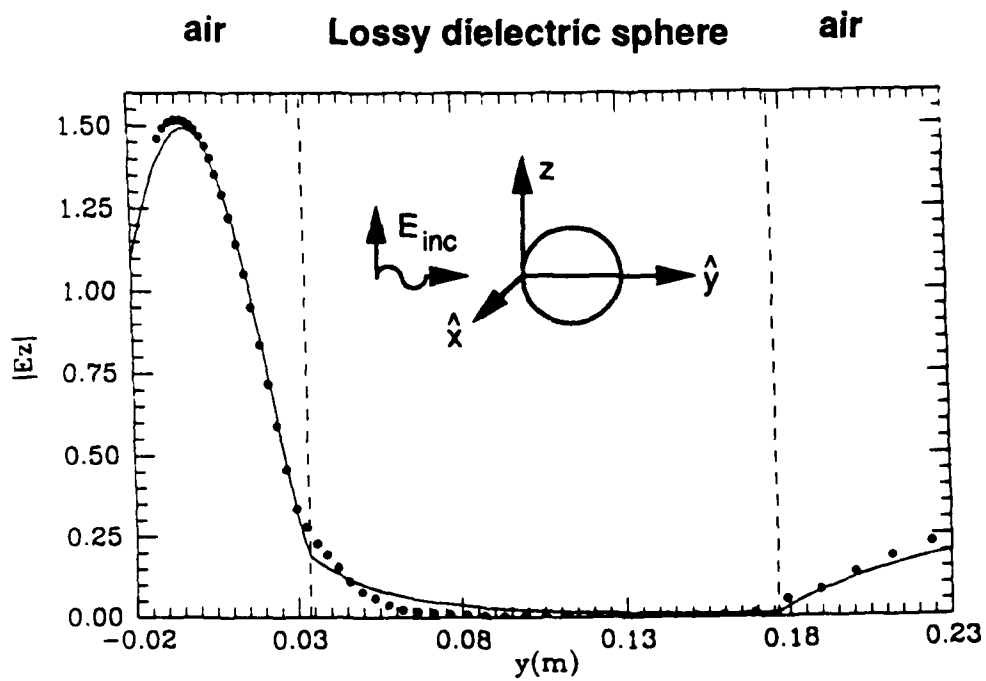
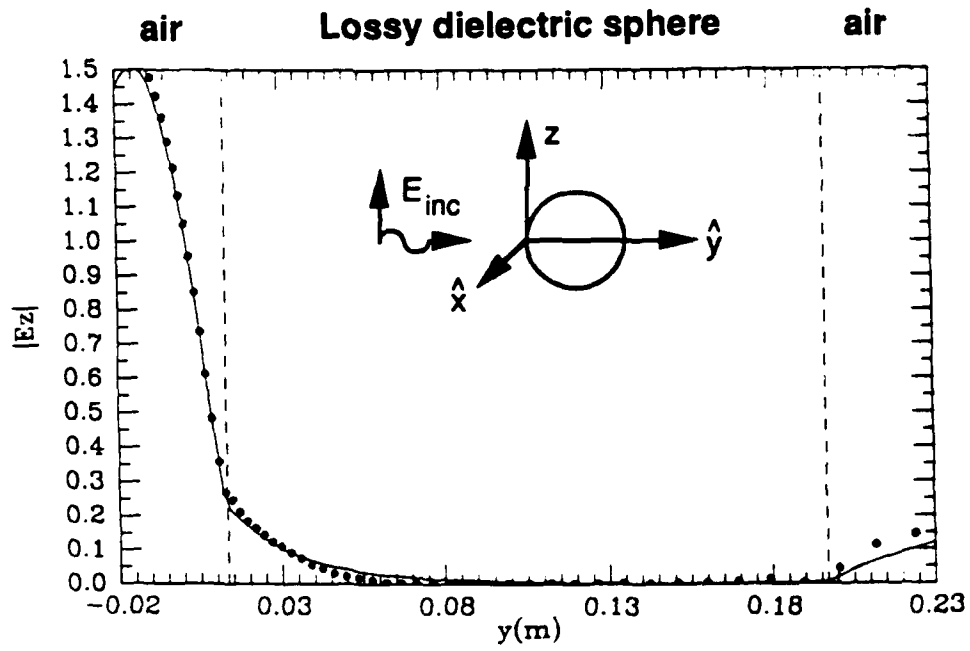


Figure 5 (continued).

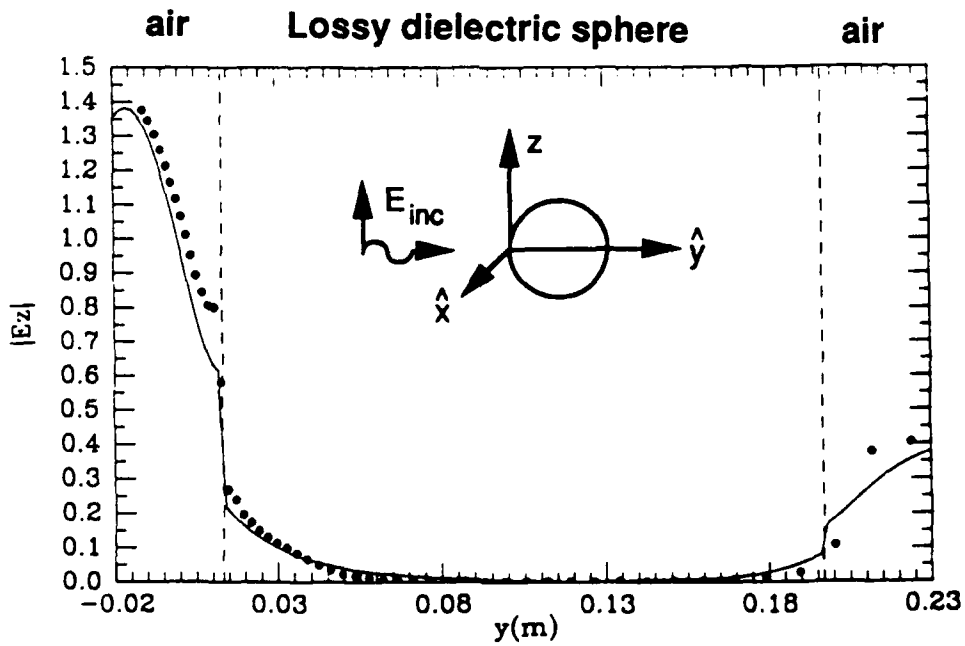
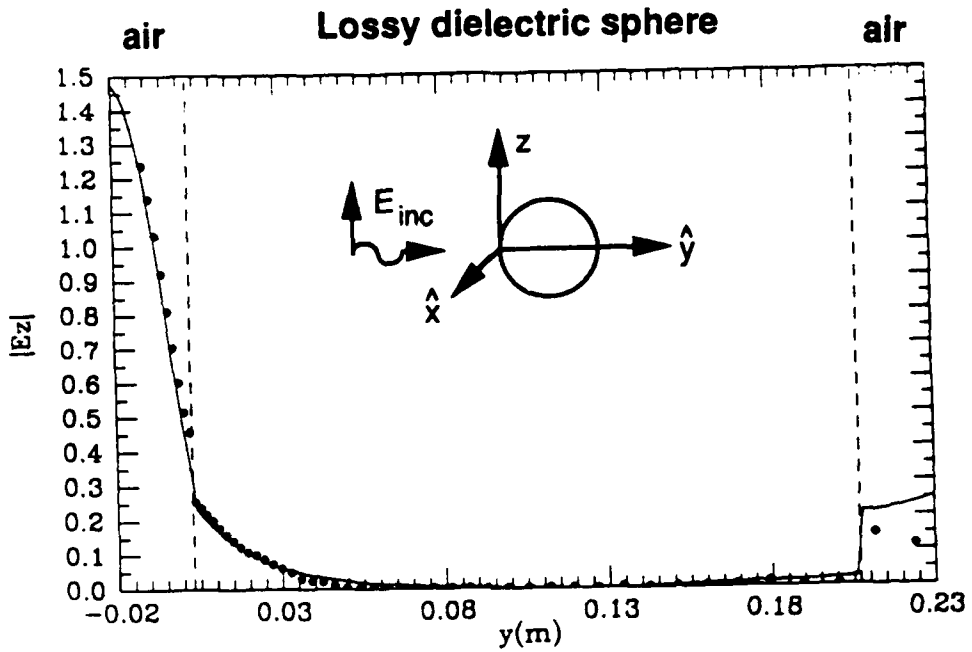


Figure 5 (continued).

1. 82,992-cell model (less than 12 Mbytes; Silicon Graphics, IRIS, APOLLO 10,000; computation time approximately 7 s per iteration)
2. 644,176-cell model (approximately 26 Mbytes; APOLLO 10,000 and IBM 520; computation time approximately 36 s per iteration on APOLLO 10,000 and about 4 s on IBM 520)
3. 1,943,700-cell model (approximately 75 Mbytes; APOLLO 10,000 with extended memory; computation time approximately 72 s per iteration)

PARALLELIZATION OF THE FDTD CODE AND ITS IMPLEMENTATION ON A DISTRIBUTED MEMORY TRANSPUTER

His work done by Professor Kris Sikorski and his student Youn-Hsin Young is described in detail [33]. As a result of this task the FDTD code has been rewritten in a parallelized C-language version and run on a distributed memory transputer array consisting of 21 T-800/20 MHz processors interconnected in linear topology and served by the APOLLO DN 10,000 workstation as a host machine (Figure 1 of [33]). For the 2.62-cm (nominal 1-in.) model, the parallelized version of the code is about six times faster than the sequential version using APOLLO 10,000. It will take a larger memory than presently available with this transputer (42 Mbytes) to run a 1.31-cm (nominal 1/2-in.) model of the human body.

WORK PROPOSED FOR NEXT YEAR

- A. With the high-resolution procedures that have now been developed, it has become imperative that we develop a higher-resolution model of the human body than the one that we are presently using. It may be recalled that the present model was developed 5-6 years ago from single-tissue properties prescribed for each 1.31 cm \times 1.31 cm area of the anatomic cross sections that were available for separations on the order of 2.3-2.7 cm. Interpolations were then used to obtain the compositions of the numerical cells for various intermediate locations.

With the possibility of using linearly expanding grids, we would like to be able to prescribe properties for cell sizes as small as 1.44 mm for dosimetric calculations at 3,000 MHz.

We would like to use a magnetic resonance imaging (MRI) tape of the human body to define the contours of the various organs and tissues for each of the cross sections of the body. If the model were kept flexible enough so that a dominant tissue could be prescribed for each of the cells likely to be on the order of a millimeter or so at higher frequencies, we could use a look-up table of only 16 tissues for all of the cells rather than the presently used compositions of the various tissues for each of the N cells representing the body. In addition to an accurate representation of the body at higher frequencies where cell sizes on the order of millimeters are needed, use of a 16-tissue look-up table would result in a considerable reduction in the memory requirement and hence the computation time for the code.

- B. We would like to investigate techniques to improve efficiency of calculations, particularly at higher frequencies where the cell size is of necessity small and hence a large number of cells are needed to represent the whole body.

At higher frequencies where the EM deposition is primarily superficial, it may be possible to bring the absorbing boundary behind the model closer to, and perhaps within, the body, thereby reducing the interaction space that is to be modeled.

A method of choice will be the use of the **linearly expanding grid** by which the exposed frontal region of the body may be expressed by a finer grid and an increasingly coarser grid used for the interior of the body. Now that this algorithm has been developed and tested with objects such as spheres (Figure 5), it should be possible to adapt it for use with the new high-resolution model of the human body that will be developed as Task A of the project.

Once the high-resolution anatomically based model of the human body has been developed, it will be our objective to develop an atlas of SAR distributions for frequencies up to 5-6 GHz using the techniques outlined here. It would thus be possible to obtain SAR distributions for the biologically sensitive regions such as the eyes, the brain, the gonads, and others, with resolutions on the order of millimeters.

For this atlas of SAR distributions for isolated and for grounded and shoe-wearing conditions, we would cover the region 10-6,000 MHz with smaller frequency separations of 10 MHz at lower frequencies increasing to as much as 200-500 MHz at the high end of the frequency band. We have talked to the personnel at the Utah Supercomputing Institute (University of Utah) who have volunteered to help us develop the computer graphical procedures to display the calculated SAR distributions. When these procedures are developed it should be possible to include computer-generated pictures of SAR distributions.

- C. Once Tasks A and B have been satisfactorily completed, we would like to use the technique thus developed to understand the coupling of the high-power microwave (HPM) pulse to the human body. The exposure parameters to use for these calculations (frequency, time domain, wave shape, etc.) will be prescribed by Dr. Erwin of the USAF School of Aerospace Medicine.

If pertinent, the nonlinearities of the tissue properties at the high-field strengths associated with HPM pulse may also be incorporated by modifying the Maxwell's equations that are solved.

- D. The data calculated for coupling of the HPM pulse will be graphically displayed for the various sections of the body by means of a videotape of a computer-generated movie.
- E. The impedance method previously developed in our laboratory [27-29] is ideally suited for calculations of induced currents and SARs for exposure to time-varying magnetic and electric fields due to electromagnetic-rail-gun type devices. We look forward to receiving the specifications of such a device from the Air Force project monitor to proceed with the calculations for the high-resolution anatomically based model of the human body.
- F. Significant progress has recently been made in developing an anatomically based thermal model of the human body [30] to calculate temperature distributions for EM exposure conditions. In this work, a computerized tomography (CT) scan-based model of the human torso has been combined with the anatomically based model for the rest of the body to obtain temperature distributions in the presence of SARs due to RFR. The model of the body consisted of about 150,000 cubic cells (0.87 cm per side), and about 450,000 air cells. Unlike the previous model, this model incorporates a skin layer which allows for a proper heat balance with the surrounding ambient. We propose to adapt this model to the SAR calculations that are now possible to about 3,000 MHz and start to obtain the temperature distributions for the RFR exposure conditions at various frequencies. Of particular interest are the power densities (or SARs) that will result in measurable changes in temperature for the various organs and the ensuing changes in the biological parameters such as blood flow and heat loss by mechanisms such as perspiration, respiration, and others.

CONCLUDING REMARKS

The major objective of this project is to develop advanced user-friendly codes with degrees of resolution that would have been unthinkable just a few years ago. The eventual goals of the project are to create an atlas of SAR distributions for the human body for RFR exposure for isolated and for grounded and shoe-wearing conditions, and the fifth edition of the RFR dosimetry handbook with emphasis on anatomically based models for SAR and temperature distributions.

MANUSCRIPT ACCEPTED FOR PUBLICATION

1. Chen, J. Y. and O. P. Gandhi. Currents induced in an anatomically based model of a human for exposure to vertically polarized EMP, to appear in IEEE Transactions on Microwave Theory and Techniques, Vol. MTT-39, January 1991.

MANUSCRIPTS IN PREPARATION

2. Gandhi, O. P., Y. G. Gu, and J. Y. Chen. Part-body and organ-averaged SAR distributions for 1.31-cm resolution, anatomically-based model of a human for plane-wave exposures 100-915 MHz, to be submitted to Health Physics.
3. Chen, J. Y. and O. P. Gandhi. A simple convolution procedure for calculating currents induced in the human body for exposure to EMP, to be submitted to IEEE Transactions on Electromagnetic Compatibility.
4. Gao, B. Q. and O. P. Gandhi. A new expanding grid algorithm for the finite-difference time-domain method, to be submitted to IEEE Transactions on Antennas and Propagation.

REFERENCES

1. ANSI C95.1-1982. American National Standard -- Safety levels with respect to human exposure to radio-frequency electromagnetic fields, 300 kHz to 100 GHz. IEEE, New York.
2. Spiegel, R. J., M. B. E. Fatmi, and K. S. Kunz. Application of a finite-difference technique to the human radio frequency dosimetry problem, *Journal of Microwave Power*, Vol. 20:241-254, 1985.
3. Spiegel, R. J., M. B. E. Fatmi, and T. R. Ward. A finite-difference electromagnetic deposition/thermoregulatory model: Comparison between theory and measurements, *Bioelectromagnetics*, Vol. 8:259-273, 1987.
4. Sullivan, D. M., D. T. Borup, and O. P. Gandhi. Use of the finite-difference time-domain method in calculating EM absorption in human tissues, *IEEE Transactions on Biomedical Engineering*, Vol. BME-34:148-157, 1987.
5. Sullivan, D. M., O. P. Gandhi, and A. Taflove. Use of the finite-difference time-domain method in calculating EM absorption in man models, *IEEE Transactions on Biomedical Engineering*, Vol. BME-35:179-186, 1988.
6. Chen, J. Y. and O. P. Gandhi. RF currents induced in an anatomically-based model of a human for plane-wave exposures 20-100 MHz, *Health Physics*, Vol. 57:89-98, 1989.
7. Chen, J. Y. and O. P. Gandhi. Electromagnetic deposition in anatomically-based model of man for leakage fields of a parallel-plate dielectric heater, *IEEE Transactions on Microwave Theory and Techniques*, Vol. MTT-37:174-180, 1989.
8. Wang, C. Q. and O. P. Gandhi. Numerical simulation of annular-phased arrays for anatomically-based models using the FDTD method, *IEEE Transactions on Microwave Theory and Techniques*, Vol. MTT-37:118-126, 1989.
9. Yee, K. S. Numerical solution of initial boundary value problems involving Maxwell's equations in isotropic media, *IEEE Transactions on Antennas and Propagation*, Vol. AP-14:302-307, 1966.
10. Taflove, A. and M. E. Brodwin. Numerical solution of steady-state electromagnetic scattering problems using the time-dependent Maxwell's equations, *IEEE Transactions on Microwave Theory and Techniques*, Vol. MTT-23:623-630, 1975.
11. Taflove, A. and M. E. Brodwin. Computation of the electromagnetic fields and induced temperatures within a model of the microwave irradiated human eye, *IEEE Transactions on Microwave Theory and Techniques*, Vol. MTT-23:888-896, 1975.
12. Taflove, A. Application of the finite-difference time-domain method to sinusoidal steady-state electromagnetic-penetration problems, *IEEE Transactions on Electromagnetic Compatibility*, Vol. EMC-22:191-202, 1980.
13. Umashankar, K. and A. Taflove. A novel method to analyze electromagnetic scattering of complex objects, *IEEE Transactions on Electromagnetic Compatibility*, Vol. EMC-24:397-405, 1982.
14. Holland, R. THREDE: A free-field EMP coupling and scattering code, *IEEE Transactions on Nuclear Science*, Vol. NS-24:2416-2421, 1977.

15. Kunz, K. S. and K-M. Lee. A three-dimensional finite-difference solution of the external response of an aircraft to a complex transient EM environment: Part 1 - The method and its implementation, *IEEE Transactions on Electromagnetic Compatibility*, Vol. EMC-20:328-332, 1978.
16. Mur, G. Absorbing boundary conditions for the finite-difference approximation of the time-domain electromagnetic field equations, *IEEE Transactions on Electromagnetic Compatibility*, Vol. EMC-23:377-382, 1981.
17. Eycleshymer, A. C. and D. M. Schoemaker. *A cross-section anatomy*. Appleton-Century-Crofts, New York, 1970.
18. Grønhaug, K. L. Measurements of EMP induced currents in the human body, Report FFI/NOTAT-88/4038, Forsvarets Forsknings-institutt, Norwegian Defense Research Establishment, Box 25-N-2007, Kjeller, Norway, 1988.
19. Guy, A. W. Analysis of time domain induced current and total absorbed energy in humans exposed to EMP electric fields, Final Report prepared for ERC Facilities Service Corporation, 3211 Germantown Road, Fairfax, VA 22030, June 30, 1989.
20. Burke, G. J. and A. J. Poggio. Numerical electromagnetics code (NEC) -- Method of moments, Lawrence Livermore National Laboratory, Livermore, CA.
21. Gandhi, O. P. State of the knowledge for electromagnetic absorbed dose in man and animals, *Proceedings of the IEEE*, Vol. 68:24-32, 1980.
22. Stuchly, M. A. and S. S. Stuchly. Dielectric properties of biological substances -- Tabulated, *Journal of Microwave Power*, Vol. 15:19-26, 1980.
23. Johnson, C. C. and A. W. Guy. Nonionizing electromagnetic wave effects in biological materials and systems, *Proceedings of the IEEE*, Vol. 60:692-718, 1972.
24. Stuchly, S. S., A. Kraszewski, M. A. Stuchly, G. W. Hartsgrrove, and R. J. Spiegel. RF energy deposition in a heterogeneous model of man: Far-field exposures, *IEEE Transactions on Biomedical Engineering*, Vol. 34:951-957, 1987.
25. Gandhi, O. P., J. Y. Chen, and A. Riazi. Currents induced in a human being for plane-wave exposure conditions 0-50 MHz and for RF sealers, *IEEE Transactions on Biomedical Engineering*, Vol. BME-33:757-767, 1986.
26. Mautz, J. R. Mie series solution for a sphere, *IEEE Transactions on Microwave Theory and Techniques*, Vol. MTT-26:375, 1978.
27. Gandhi, O. P., J. F. DeFord, and H. Kanai. Impedance method for calculation of power deposition patterns in magnetically-induced hyperthermia, *IEEE Transactions on Biomedical Engineering*, Vol. BME-31:644-651, 1984.
28. Gandhi, O. P. and J. F. DeFord. Calculation of EM power deposition for operator exposure to RF induction heaters, *IEEE Transactions on Electromagnetic Compatibility*, Vol. EMC-30:63-68, 1988.
29. Orcutt, N. and O. P. Gandhi. A 3-D impedance method to calculate power deposition in biological bodies subjected to time-varying magnetic fields, *IEEE Transactions on Biomedical Engineering*, Vol. BME-35:577-583, 1988.

30. Orcutt, N. and O. P. Gandhi. Use of bioheat equation to calculate temperature in a human body for hyperthermia with capacitive plate electrodes, Paper presented at the Twelfth Annual Meeting of the Bioelectromagnetics Society, San Antonio, Texas, June 10-14, 1990.
31. Chen, J. Y. and O. P. Gandhi. Currents induced in an anatomically based model of a human for exposure to vertically polarized EMP, IEEE Transactions on Microwave Theory and Techniques, Vol. MTT-39:31-39, January 1991.
32. Gandhi, O. P., Y. G. Gu, and J. Y. Chen. SAR and induced current distributions in anatomically based models of a human for plane-wave exposures at frequencies 20-915 MHz, manuscript in preparation.
33. Sikorski, K. and Y. H. Young. Distributed implementation of the FDTD method for automated radio frequency dosimetry, manuscript in preparation.